In situ study of the metal–insulator transition in VO_2 by EELS and ab initio calculations

F. Espinosa-Magaña, Alberto Rosas, H.E. Esparza-Ponce, M.T. Ochoa-Lara, A. Aguilar-Elguezabal

Changes in the dielectric properties during the thermochromic transition of commercial VO_2 powders were determined *in situ*, by analyzing the low-loss region of the electron energy-loss spectroscopy (EELS) spectra in a transmission electron microscope at room temperature (insulator phase) and 100 8C (metallic phase). A comparison of experimental EELS spectra and *ab initio* density-functional theory calculations (WIEN2k code) within the generalized gradient approximation (GGA) is presented. A characteristic peak around 5.6 eV appears in the energy-loss function in metallic phase, which is absent in insulator phase. The origin of the characteristic peak is analyzed by means of energy-band structure calculations.

Vanadium oxides are found in many different stoichiometries (VO, VO_2, V_2O_3, V_2O_5, among others), and most of them undergo metal–insulator transitions with a change in temperature, sometimes accompanied by crystal structure changes during the transition. The most studied compound is certainly VO_2, which undergoes a first-order metal–insulator transition around T_c = 68 8C from high-temperature metallic phase (tetragonal structure, rutile-type) to a low-temperature insulator phase (monoclinic structure). In the last decades, this compound has been extensively studied and has come of interest because it presents remarkable changes in optical properties (thermochromic effect) during the transformation at the critical

temperature, allowing it to be used as an intelligent window coating, which can be used to control solar energy transmission.

Experimental studies on this compound include photoemission (Bermudez et al., 1992; Goering et al., 1997) and X-ray absorption (Abbate et al., 1991; Mossanek and Abbate, 2005). The optical properties of VO_2 were studied using reflectivity and transmission methods (Verleur et al., 1968; Gavini and Kwan, 1972), and more recent studies included detailed reflectivity, electron energy-loss spectroscopy (EELS), and optical conductivity measurements (Shin et al., 1990; Okazaki et al., 2004; Rozenberg et al., 1995), as well as infrared spectroscopy and nano-imaging (Qazilbash et al., 2007). From a theoretical point of view, a number of first principles calculations have been carried out for VO_2 by several methods, including local density approximation (LDA) (Wentzcovitch et al., 1994; Mossanek and Abbate, 2007), as well as the cluster model methods (Uozumi et al., 1993), and LMTO band-structure calculations (Kurmaev et al., 1998). The microscopic origin of the metal to insulator transition in VO_2 was also studied using the dynamical mean field theory (DMFT) method (Laad et al., 2006). EELS has been widely used in the study of materials composition and electronic structure (Egerton, 1996; Ahn, 2004; Brockt and Lakner, 2000). The interactions of fast electrons with the specimen result in electrons being excited into unoccupied energy levels within the conduction band, as well as collective excitation of valence electrons. From the dielectric theory, it is possible to relate the experimental single scattering distribution $S(E)$ to the energyloss function $\mathrm{Im}(-1/\epsilon)$ (Egerton, 1996), by:

$$S(E) = \frac{I_0 t}{\pi a_0 m_0 v^2} \mathrm{Im}\left[-\frac{1}{\varepsilon(q,E)}\right] \ln\left[1 + \left(\frac{\beta}{\theta_E}\right)^2\right] \qquad (1)$$

where $\varepsilon(q,E) = \varepsilon_1 + i\varepsilon_2$ is the complex dielectric function at energy-loss E and momentum transfer q, a_0 the Bohr radius, m_0 the electron rest mass, υ the electron beam velocity, θ the scattering angle and is the characteristic scattering angle, θ_E is $= E/(\gamma m_0 v^2)$ is the characteristic scattering angle, γ is he relativistic factor, I_0 is the zero-loss intensity, t the specimen thickness, and b is the collection semi-angle. The real and imaginary parts of the dielectric function can be obtained from the energy-loss function through Kramers–Kronig analysis.

EELS has been widely applied in fingerprint studies, allowing the identification of phases by comparing well-known spectra. In the high-loss region, analysis of the first 10 eV of the spectra after the ionization edge (ELNES) can give information about the oxidation state, absolute energy position, and local symmetry via d level splittings in transition metal elements and orbital hybridization. The low-loss region can provide information about composition and electronic structure, as well as optical properties, although it has not been as widely applied as ELNES. The reason is due to the well-known fact that low-losses are caused by all possible transitions between the valence band and the conduction band. The valence band is made up of dispersed levels as opposed to almost flat core levels, and the interpretation of EELS is a priori more difficult.

In this work, we studied the changes in electronic structure associated with the thermochromic transition in VO_2 with both EELS and *ab initio* calculations with the FLAPW method, as implemented in WIEN2k code (Blaha et al., 1990, 2001). We

focus on the experimental characteristic peak at around 5.6 eV in the energy-loss function, which is more intense in the metal (tetragonal) phase than in the insulator (monoclinic) phase, thus allowing the identification of phases. Identification of the transition temperature is carried out by differential scanning calorimetry (DSC), and the phase identification is accomplished by X-ray diffractometry (XRD) studies.

The justification for this article is that, even though there has been considerable work involving both experimental and theoretical methods on VO_2, there have been very few studies relating *ab initio* calculations with electron energy-loss spectra acquired in the electron microscope, and most of all, *in situ* studies of phase transformations are not a common issue in the literature. We found it useful and interesting to carry out the study on commercial polycrystal powders, instead of single crystals used in most of the previous studies. Commercial powders are easier to manipulate, and much cheaper than single crystals, whose fabrication is quite expensive.

Experimental

Commercial VO_2 powders (Sigma Aldrich 99% pure) have been used. DSC measurements were carried out in a TA Instruments DSC 2926 modulate apparatus under inert (Ar) atmosphere using an aluminum crucible and Argon flux, from 20 to 140 8C at a heating rate of 5 8C min^{-1}.

To check that the correct phases were obtained, the phase transition in this commercial VO2 powders were analyzed in situ by XRD in the diffractometer Siemens D5000, using the Cu Ka radiation. The temperatures used were 50, 70 and 100 8C.

Thin suitable samples for transmission electron microscopy were prepared by placing clean, dry crushed powders onto commercial folding copper grids. To obtain

EELS spectra from both phases, the thermochromic transition was induced by placing the sample in a heating sample holder, and EELS spectra were acquired at room temperature and 100 8C, corresponding to insulator (monoclinic) and metallic (tetragonal) phases, respectively. In this way, we generated an in situ heating process that allowed us to obtain spectra for the two phases in the same region of the sample.

Electron energy-loss spectra were obtained using a Gatan parallel electron energy-loss spectrometer (PEELS model 766) attached to a transmission electron microscope (TEM) Philips CM200. Spectra were acquired in diffraction mode with 0.1 eV/ channel dispersion, an aperture of 2 mm, and a collection semiangle of about 2.7 mrad. The resolution of the spectra was determined by measuring the full-width at half-maximum (FWHM) of the zero-loss peak, and this was typically close to 1.0 eV, when the TEM was operated at 200 kV. EELS spectra were corrected for dark current and readout noise. The channel to channel gain variation was minimized by normalizing the experimental spectrum with independently obtained gain spectrum of the spectrometer. Next, all spectra were deconvoluted by the zero-loss peak (ZLP) recorded in a hole of the grid to obtain single scattering distributions $S(E)$, and finally multiple plural scattering was eliminated by applying the Fourier-log deconvolution process.

Calculation details

Self-consistent band structure calculations were performed using density-functional theory (DFT) with the full-potential linearized augmented plane-wave (FLAPW) method, using the WIEN2k code (Blaha et al., 2001).

Exchange and correlation were treated using the generalized gradient approximation (GGA) for the potential. The core states were treated in a fully relativistic fashion. The wave functions within the muffin-tin spheres were expanded in spherical harmonics with an angular momentum up to l = 10. Additional local orbital extensions were used to avoid linearization errors. Non-spherical contributions to the charge density and the potential within the muffin-tin spheres were considered up to l_{max} = 4. In the interstitial region, plane waves with reciprocal lattice vectors up to G = 10 were included, and the plane-wave cut-off ($R_{MT}K_{max}$) was set to 7. Self-consistency was considered to be achieved when the total energy variation from iteration to iteration did not exceed 10^{-6} Ry, on a mesh containing 396 (336) k-points in the irreducible Brillouin zone (IBZ) for the monoclinic (tetragonal) phase.

The dielectric function can be obtained from the OPTIC Program of the WIEN2k code (Ambrosch-Draxl and Sofo, 2006), allowing for comparison with experiment:

$$\varepsilon_{2ii}(\omega) = \frac{4\pi^2 e^2}{m^2\omega^2 V}\sum_{v,c,k}\left|\langle\psi_k^v|\, p_i\,|\psi_k^c\rangle\right|^2 \times \delta(E_{\psi_k^c} - E_{\psi_k^v} - \hbar\omega) \qquad (2)$$

Matrix elements are calculated from the electron states and integration over the irreducible Brillouin zone is performed to calculate the imaginary part of the dielectric function. Then a

Kramers–Kronig analysis is performed to obtain the real part of the dielectric function ε_1, and finally, the energy-loss function $\mathrm{Im}(-1/\varepsilon)$. In anisotropic materials, dielectric properties must be described by the dielectric tensor which, by symmetry

considerations in tetragonal structures, reduces to only two independent components $\varepsilon_{xx} = \varepsilon_{yy}$ and ε_{zz}. In monoclinic structures, all three components should be considered.

The crystal structure of VO_2 in the monoclinic and tetragonal phases has been widely studied experimentally. The monoclinic structure belongs to the space group $P21/c$. The lattice constants are a = 5.743, b = 4.517, c = 5.375 Å and b = 122.56§, taken from the experimental results (Mossanek and Abbate, 2007). The atomic positions are: V at (0.233, 0.024, 0.021) and two non-equivalent oxygen atoms at (0.882, 0.288, 0.272) and (0.300, 0.315, 0.293). The tetragonal phase, with space group $P42/mnm$ has lattice parameters, taken from experimental data (Mossanek and Abbate, 2007), a = 4.53 and c = 2.896 Å. The atomic positions are: V at (0, 0, 0) and O at (0.305, 0.305, 0).

The optical properties were calculated on a mesh containing 3744 (3400) k-points in the irreducible part of the Brillouin zone for the monoclinic (tetragonal) phase, as many points are needed for optical calculations.

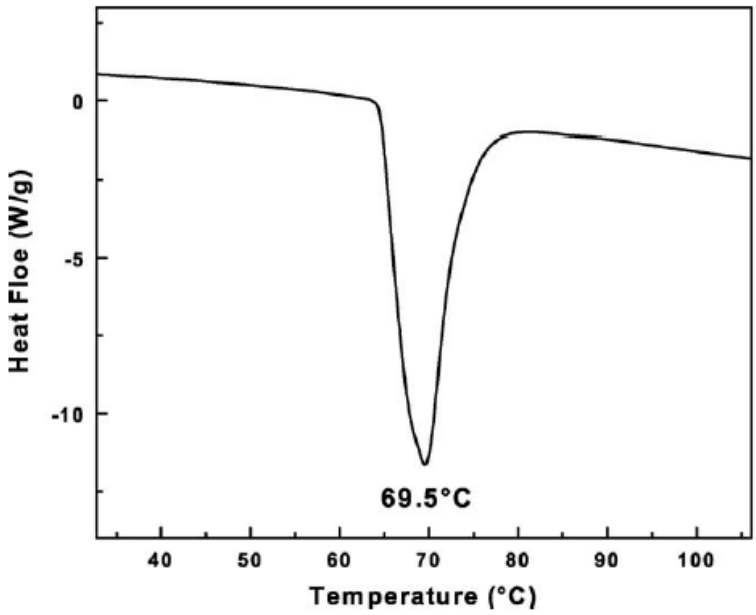

Fig. 1. DSC analysis of VO_2 powders, heated under argon atmosphere.

Results and discussion

The DSC of the VO2 powders is shown in Fig. 1, where a thermochromic phase transition is observed, and characterized by an endothermic broad peak with a minimum at 69.5 8C. This firstorder transition can be attributed to the monoclinic to tetragonal phase change, as confirmed by XRD. The transition temperature found at 69.5 8C is higher than the value previously reported of about 68 8C, and we believe this discrepancy may be due to impurities in the VO2 powders (99.9% purity).

Fig. 2 shows the evolution of the VO2 X-ray diffraction patterns at room temperature and 70 8C, acquired by placing the sample in a heating crucible. The characteristic peak at 2u = 27.868, and coming from reflections (2 0 1), belongs to VO2 monoclinic structure, which is a stable phase at room temperature. After raising the temperature at 70 8C, the characteristic peak transforms to the (1 0 0) reflection peak, coming from the VO2 tetragonal structure with a characteristic peak at 2u =

27.678.

Fig. 3 shows a zoom of the region where phase transformation takes place, where the graphs have been shifted up for clarity. We have included a diffraction pattern at 100 8C, to corroborate that

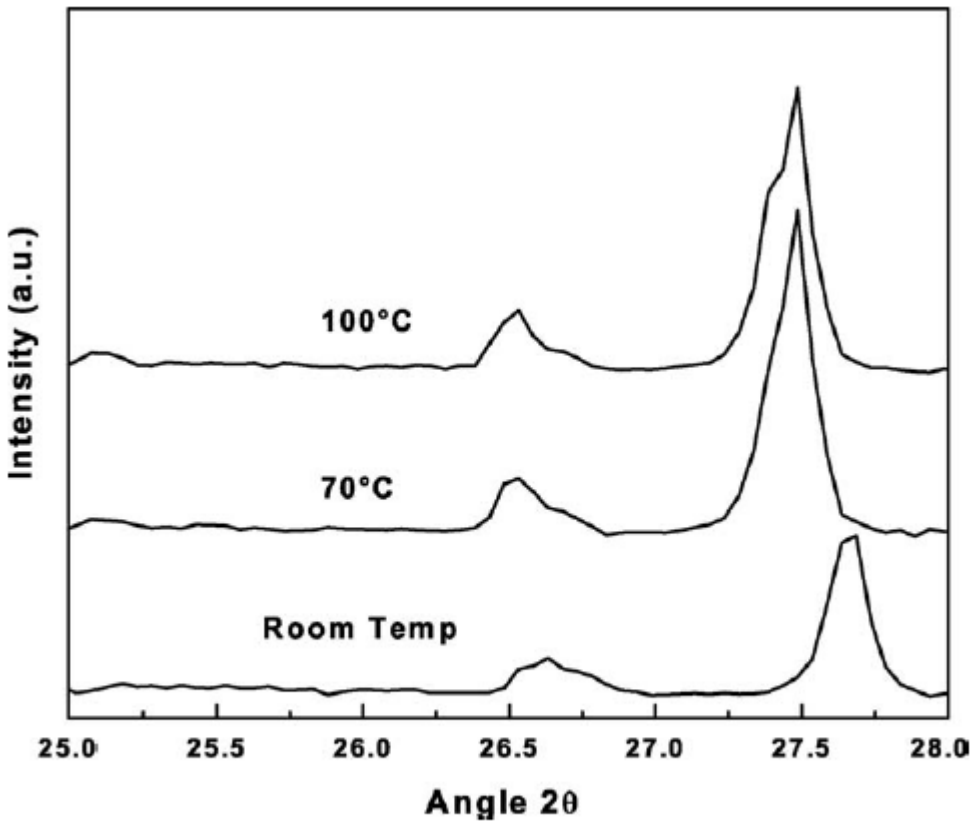

Fig. 3. Zoom of diffraction patterns at room temperature (insulating), 70 8C (metallic) and 100 8C (metallic) at 2u value where thermochromic transition takes place.

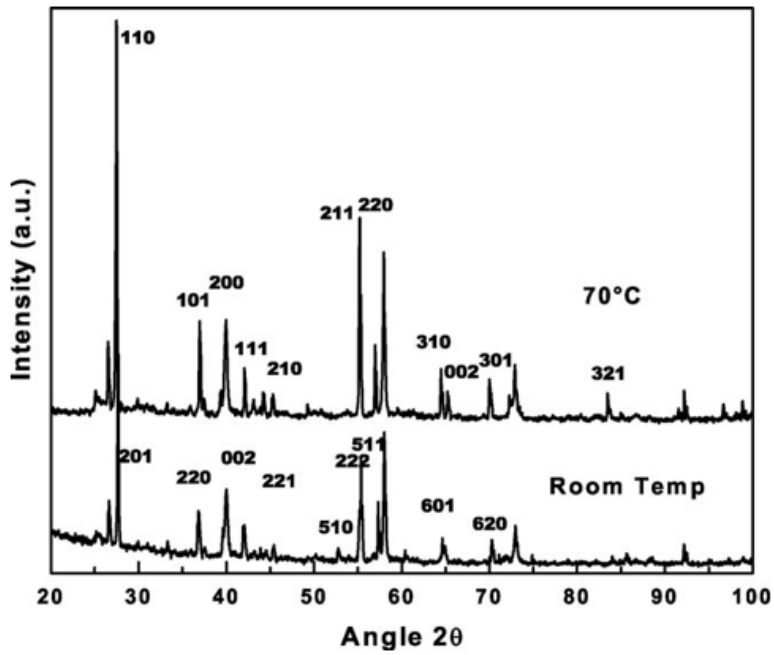

Fig. 2. Diffraction patterns at room temperature (insulating) and 70 8C (metallic).

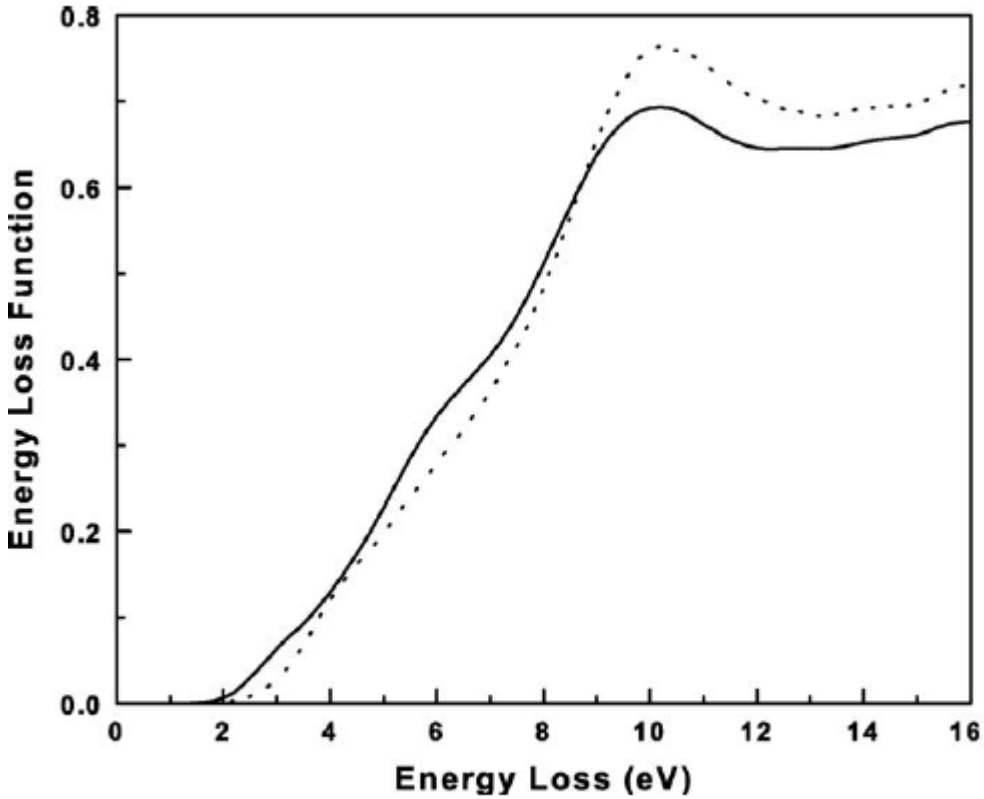

Fig. 4. EELS spectra of VO_2 at room temperature (· · ·), and 100 8C (—), monoclinic and tetragonal phases, respectively.

the shift of the characteristic peak is not an effect produced by heating the sample. Indeed, there is no difference between diffraction patterns at 70 and 100 ßC.

Fig. 4 shows the EELS derived energy-loss function Im($-1/\varepsilon$) of

VO_2 for monoclinic and tetragonal (rutile-type) structures, acquired at room temperature and 100 ßC, respectively. Besides the plasmon peaks, observed at 10.2 eV for both phases, a clearly observed difference between the two structures exists, where the rutile phase has a broad bump around 5.6 eV, noticeably enough to distinguish from the monoclinic phase. This can be attributed to an interband transition, as can be seen from *ab initio* calculations. Fig. 5 shows the calculated energy-loss function for VO_2 in monoclinic and tetragonal structures, along x, y and z directions, where a Lorentzian broadening, with a width of 0.5 eV, has been applied. It is observed that, although we did not acquire EELS spectra from a single crystal, we can identify the experimental spectra with the calculated one along y-direction. Even though an

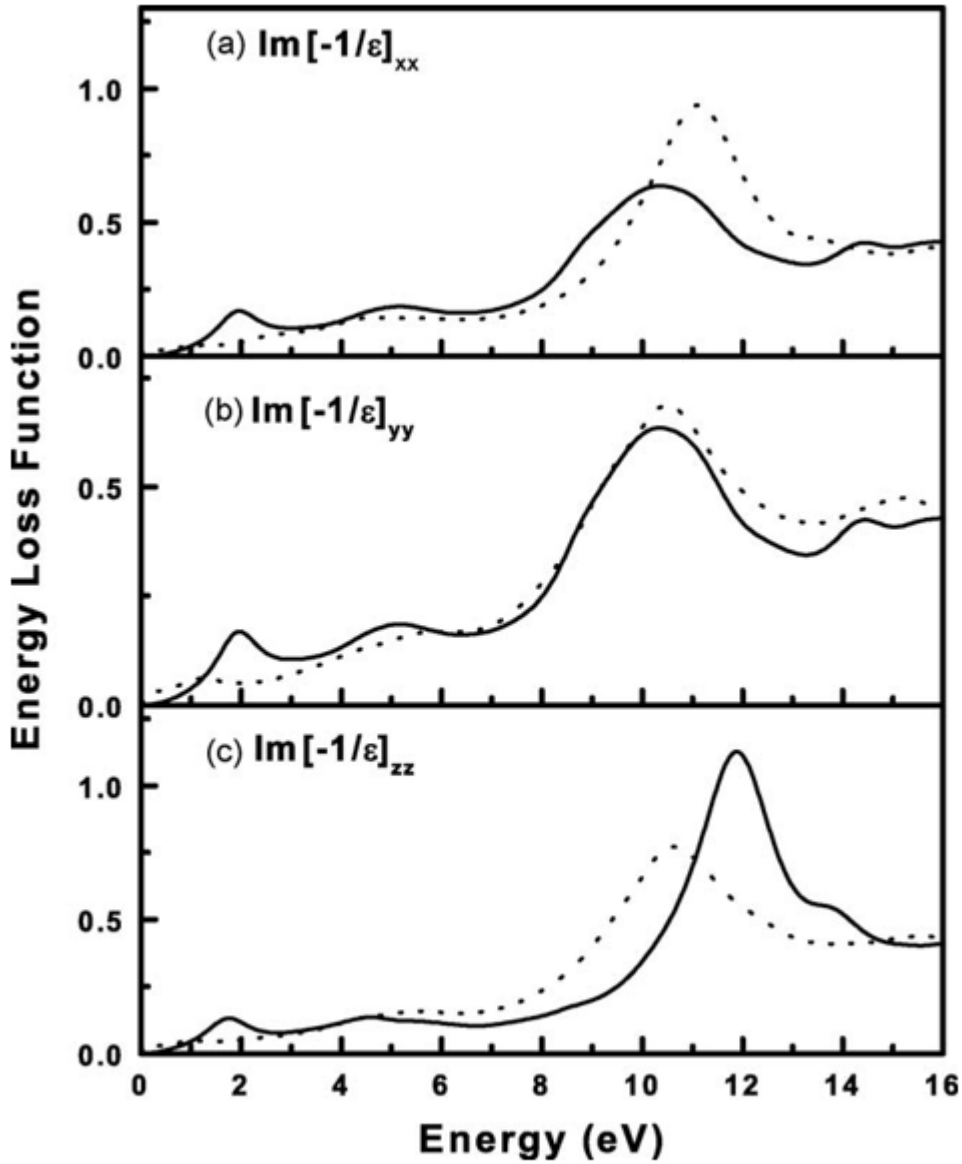

Fig. 5. Calculated: (a) *x*-, (b) *y*- and (c) *z*-components of the energy-loss function of monoclinic (·· ·) and tetragonal (—) structures.

average over the three directions is customarily done when using powders, in this case the averaged energy-loss function does not fit the experimental one, and we believe this is due to the fact that we probed mainly a small single crystal in the y-direction, given the narrow beam used in the electron microscope. In the general case, a weighted average should be taken in order to reproduce the experimental spectrum.

The $x$and y-components of the energy-loss function of the tetragonal phase have well-defined maxima at 2.0, 5.2 and 10.4 eV, whereas for the z-component well-defined maxima are found at 1.8, 4.6 and 11.9 eV. The monoclinic phase has well-defined maxima in the energy-loss function at 11.1, 10.5 and 11.9 eV for the x-, $y$and z-directions, respectively. It is clear that the $y$components of the calculated energy-loss function of tetragonal and monoclinic structures resemble those of the experimental results in Fig. 4, in both shape and intensity, except for the peak at 2 eV that is not present in the experimental spectrum. This is caused by the process for removing the zero-loss peak. Because of our energy resolution, we cannot have a reliable single scattering distribution for energies below 3 eV.

Figs. 6 and 7 show the calculated, and broadened by a Lorentzian with 0.5 eV width, real and imaginary parts of the dielectric function for tetragonal and monoclinic phases, respectively. ε_1 has zero-crossing of the energy axis with positive slope at 9.8 eV in monoclinic structure, whereas for tetragonal structure ε_1 has zero-crossing with positive slope at 1.8 and

9.4 eV. Therefore, the monoclinic structure has one well-defined plasmon oscillation at 9.8 eV and the rutile phase presents two well-defined plasmons at 1.8 and 9.4 eV. The plasmon peak at

1.8 eV is quite close to the zero-loss peak in the EELS spectra to be observed with the attained resolution, because of limitations introduced in removing the zero-loss peak. This peak has been reported previously (Abe et al., 1997). We focus our attention at the peak at 5.6 eV in the experimental energy-loss function,

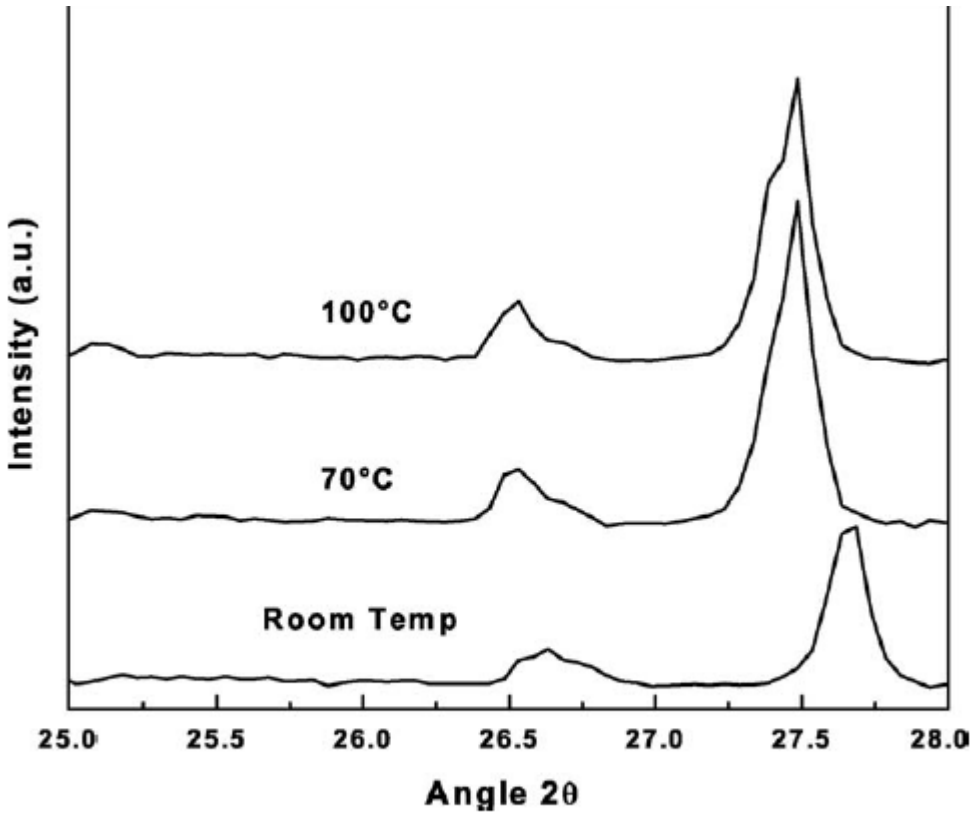

Fig. 3. Zoom of diffraction patterns at room temperature (insulating), 70 8C (metallic) and 100 8C (metallic) at 2u value where thermochromic transition takes place.

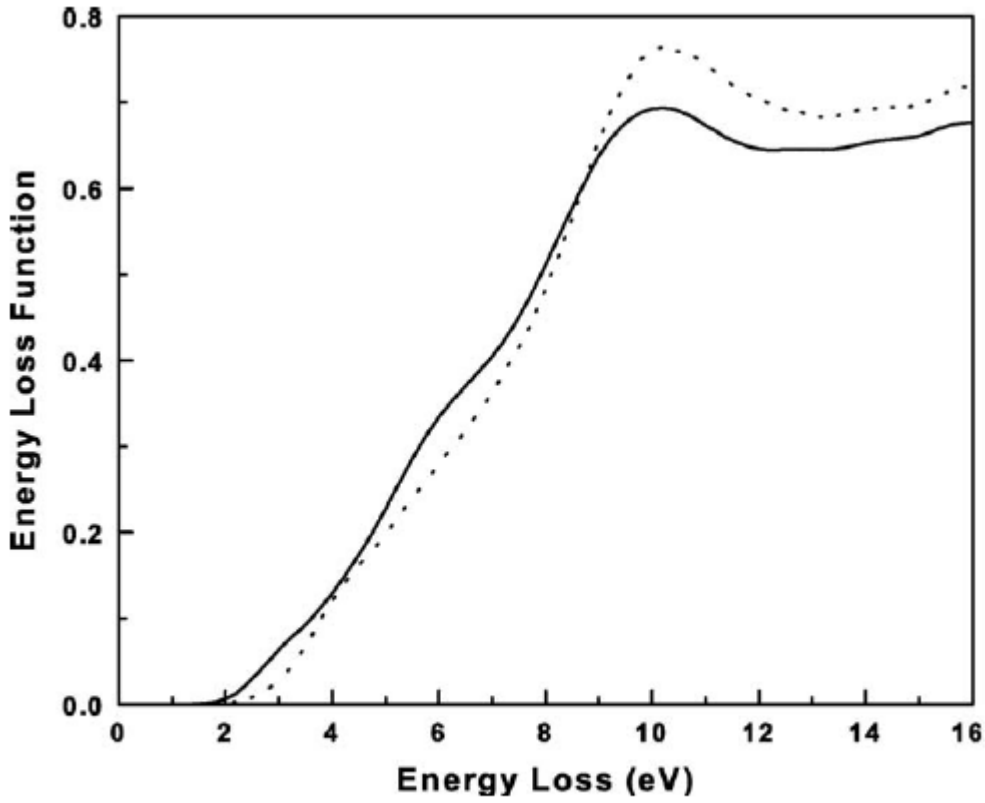

Fig. 4. EELS spectra of VO_2 at room temperature (· · ·), and 100 8C (—), monoclinic and tetragonal phases, respectively.

allowing for phase identification even at energy resolutions around 1 eV.

The featured peak at 5.2 eV, in the calculated y-component of the energy-loss function of the rutile phase, is caused by the peak at 7.0 eV in the imaginary part of the dielectric function. The origin of this peak can be sought after by calculating the partial imaginary part of the dielectric function, as implemented in WIEN2k. This allows using a smaller set of energy-bands from where the construction of the partial e_2 could be made up and which arises from all possible combinations of the valence and conduction bands of the chosen set (Launay et al., 2004; Gallegos-Orozco et al., 2008). By this method we can trace the origin of the peaks in e_2, mainly coming from transitions between bands 41 and 63 in

monoclinic structure and between bands 24 and 34 in rutile structure. Band 41 contains states in the energy interval between

−4.1 and −3.1 eV; band 63 is in the interval between 2.6 and

3.6 eV; band 24 between −3.5 and −1.8 eV; band 34 between 3.5 and 5.1 eV.

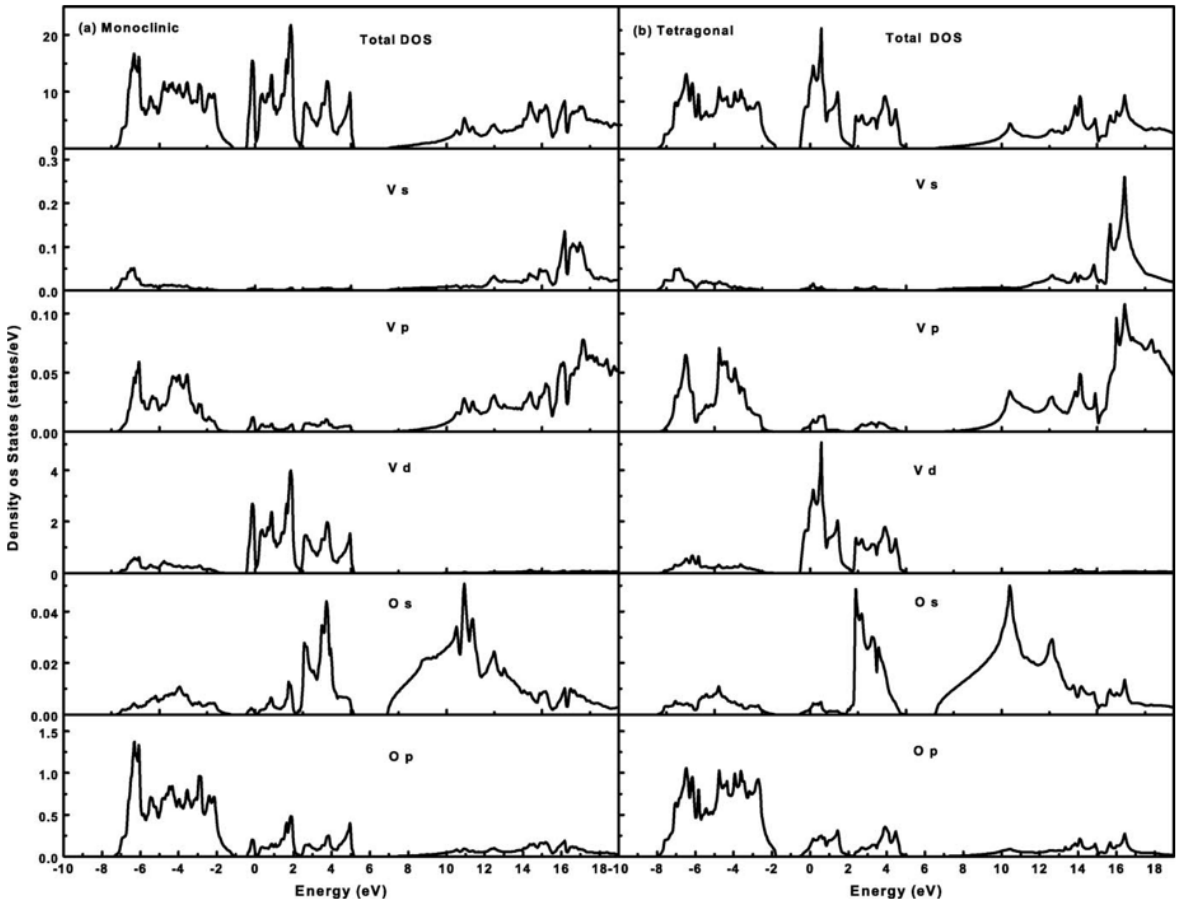

Fig. 8. Calculated total and partial density of states: (a) monoclinic and (b) tetragonal structures.

In order to get more insight into the origin of the characteristic peaks of the imaginary part of the dielectric function ϵ_2, at 7.0 an 6.6 eV in metallic and insulator phases, respectively, we calculated the total and partial densities of states (DOSs), as shown in Fig. 8, where the Fermi energy (E_F) has been chosen at the origin on the energy axes. The total DOSs are quite similar for both phases, except for the value of the DOS at the Fermi energy. The total DOS for tetragonal structure at E_F is 6.87

and 3.17 states/eV for the monoclinic structure. The difference can be attributed to the metallic character of the tetragonal phase. Even though it is well-known that DFT cannot reproduce the band-gap correctly and a rigid band shift (scissor correction) has not been applied in these calculations, the results show qualitatively the metal–insulator transition. With the help of the partial density of states, we can identify band 24 in the tetragonal structure and band 41 in the monoclinic structure as composed mainly by O 2p orbitals, while band 34 in the tetragonal structure and band 63 in the monoclinic structure are composed mainly by V 3d orbitals.

Once we know the bands giving rise to the characteristic peaks, these bands can be identified in an energy-band plot. Referring to Eq. (2), we see that the electronic structure available in the low-loss EELS spectra is related to the occupied and unoccupied electron density of states, the so-called joint density of states (JDOS) and to the matrix elements. The JDOS is

high for energies at which two energy surfaces lie parallel to one another at a particular k point in reciprocal space. At such points one has the so-called critical points. As single electron interband transitions depend on critical points in the band structure, peaks in the imaginary part of the dielectric function are caused by the presence of critical points in the energy-band structure.

Figs. 9 and 10 show the calculated band structures for monoclinic and tetragonal phases, respectively, where the transitions between the bands 41 and 63 in the monoclinic structure and between bands 24 and 34 in the tetragonal structure, have been identified at the high symmetry G point. These transitions are indicated with an arrow and the bands are shown in thicker lines. Transitions in both phases

occur between O 2p and V 3d orbitals.

Because of the density of states is not very different in the two structures, the difference between the ϵ_2 spectra comes from the matrix elements, at least around 5.2 eV. This is particularly

important because the difference characterizing the two phases lies in this energy region.

It is frequently addressed in the literature that, assuming the matrix elements are constant, peaks in the imaginary part of the dielectric function available in a low-loss EELS spectrum, can be related to maxima in the density of states. However, in this case, this assumption would give rise to erroneous interpretations.

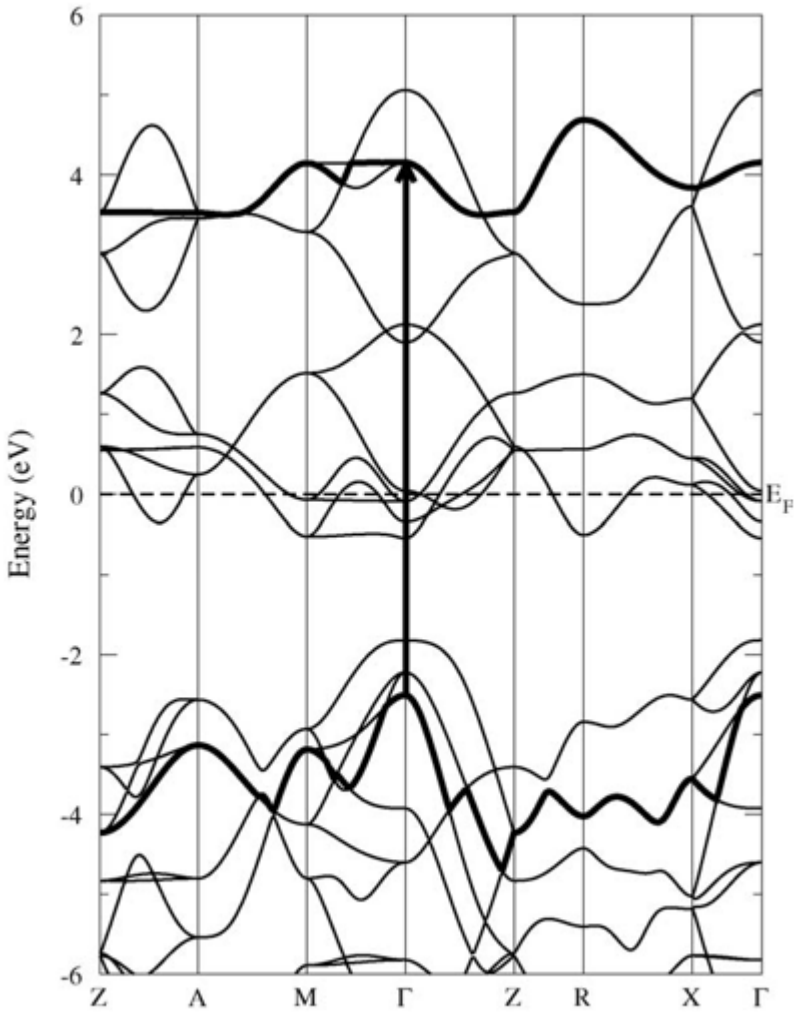

Fig. 9. Calculated energy-band structure of metallic (tetragonal) VO_2. The arrow indicates the transition giving rise to the 7.0 eV peak in ε_2.

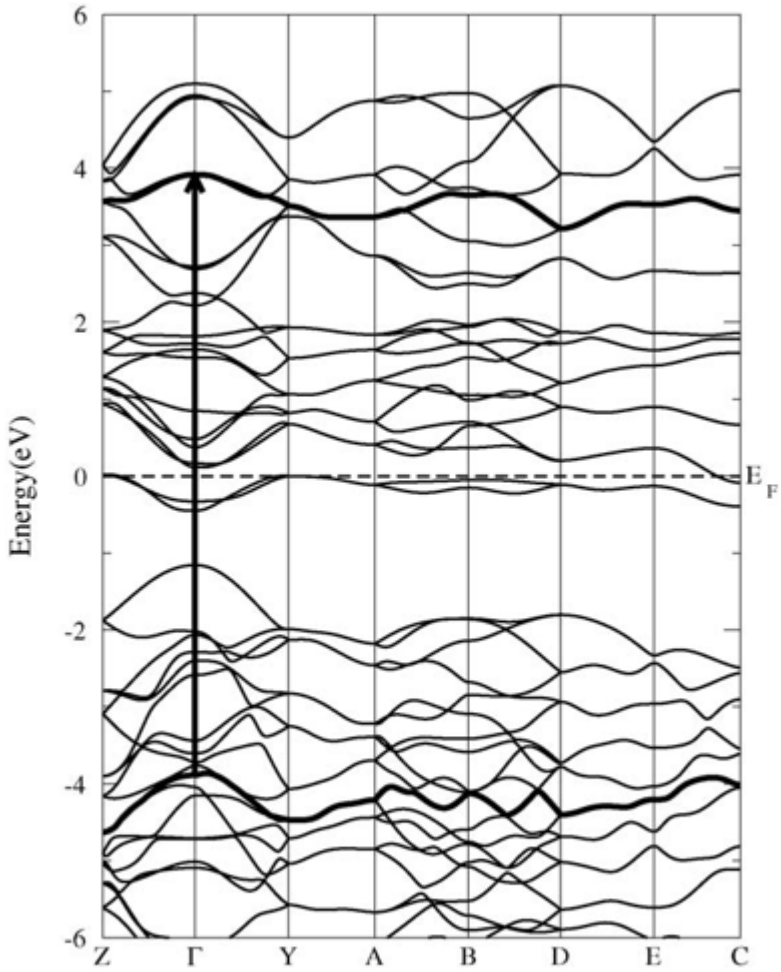

Fig. 10. Calculated energy-band structure of insulating (monoclinic) VO_2. The arrow indicates the transition giving rise to the 6.6 eV peak in ε_2.

Conclusions

The metal–insulator transition of VO_2 has been studied *in situ* by low-loss electron energy-loss spectroscopy. Spectra were acquired at room temperature and 100 8C, corresponding to insulator (monoclinic) and metallic (tetragonal) phases, respectively. Results for the energy-loss function show a well-defined characteristic peak

de Groot, F.M.F., Fuggle, J.C., Ma, Y.J., Chen, C.T., Sette, F., Fujimori, A., Ueda, Y., Kosuge, K., 1991. Soft-X-ray-absorption studies of the electronicstructure changes through the VO2 phase transition. Phys. Rev. B 43, 7263.

Abe, H., Terauchi, M., Tanaka, M., Shin, S., Ueda, Y., 1997. Electron energy-loss spectroscopy study of the metal–insulator transition in VO2. Jpn. J. Appl. Phys. 36, 165.

Ahn, C.C., 2004. Transmission Electron Energy Loss Spectrometry in Materials Science and the EELS Atlas. Wiley-VCH Verlag GmbH & Co. KGaA, Weinheim. Ambrosch-Draxl, C., Sofo, J.O., 2006. Linear optical properties of solids within the full-potential linearized augmented planewave method. Comput. Phys. Commun. 175, 1–14.

Bermudez, V.M., Williams, R.T., Long, J.P., Reed, R.K., Klein, P.H., 1992. Photoemission study of hydrogen adsorption on vanadium dioxide near the semiconductor–metal phase transition. Phys. Rev. B 45, 9266.

Blaha, P., Schwarz, K., Madsen, G.K.H., Kvasnicka, D., Luitz, J., 2001. Computer Code WIEN2k. Technische Universitä t Wien, Austria.

Blaha, P., Schwarz, K., Sorantin, P., Trickey, S.B., 1990. Comput. Improved version of P. Blaha, K. Schwarz, P. Sorantin and S.B. Trickey. Phys. Commun. 59, 399.

Brockt, G., Lakner, H., 2000. Nanoscale EELS analysis of dielectric function and bandgap properties in GaN and related materials. Micron 31, 435–440.

Egerton, R.F., 1996. Electron Energy Loss Spectroscopy in the Electron Microscope. Plenum Press, New York.

Gallegos-Orozco, V., Martínez-Sá nchez, R., Espinosa-Magaña, F., 2008. *In situ* characterization of the ferroelectric transition in BaTiO3 by EELS and comparison with *ab initio* methods. Phys. Rev. B 77, 045128.

Gavini, A., Kwan, C.C.Y., 1972. Optical Properties of VO2 between 0.25 and 5 eV. Phys. Rev. B 5, 3138.

Goering, E., Schramme, M., Muller, O., Barth, R., Paulin, H., Klemm, M., denBoer, M.L., Horn, S., 1997. LEED and photoemission study of the stability of VO2s surfaces. Phys. Rev. B 55, 4225.

Kurmaev, E.Z., Cherkashenko, V.M., Yarmoshenko, Yu, M., Bartkowski, S., Postnikov, A.V., Neumann, M., Duda, L.-C., Guo, J.H., Nordgren, J., Perelyaev, V.A., Reichelt, W.J., 1998. Electronic structure of VO2 studied by X-ray photoelectron and X-ray emission spectroscopies. J. Phys.: Condens. Matter 10, 4081.

Laad, M.S., Craco, L., Muller-Hartmann, E., 2006. Metal–insulator transition in rutilebased VO2. Phys. Rev. B 73, 195120.

Launay, M., Boucher, F., Moreau, P., 2004. Evidence of a rutile-phase characteristic peak in low-energy loss spectra. Phys. Rev. B 69, 035101.

Mossanek, R.J.O., Abbate, M., 2005. Evolution of the djj band across the metal–

insulator transition in VO2. Solid State Commun. 135, 189.
Mossanek, R.J.O., Abbate, M., 2007. Optical response of metallic and insulating VO2
calculated with the LDA approach. J. Phys.: Condens. Matter 19, 346225.
Okazaki, K., Sugai, S., Muraoka, Y., Hiroi, Z., 2004. Role of electron–electron and electron–phonon interaction effects in the optical conductivity of VO2. Phys. Rev. B 73, 165116.
Qazilbash, M.M., Brehm, M., Chae, B.-G., Ho, P.C., Andreev, G.O., Kim, B.-J., Yun, S.J.,
Balatsky, A.V., Maple, M.B., Keilmann, F., Kim, H.-T., Basov, D.N., 2007. Mott transition in VO2 revealed by infrared spectroscopy and nano-imaging. Science 318, 1750.
Rozenberg, M.J., Kotliar, G., Kajueter, H., Thomas, G.A., Rapkine, D.H., Honig, J.M., Metcalf, P., 1995. Optical conductivity in Mott–Hubbard systems. Phys. Rev. Lett. 75, 105.
Shin, S., Suga, S., Taniguchi, M., Fujisawa, M., Kanzaki, H., Fujimori, A., Daimon, H., Ueda, Y., Kosuge, K., Kachiet, S., 1990. Vacuum-ultraviolet reflectance and photoemission study of the metal–insulator phase transitions in VO2, V6O13, and V2O3. Phys. Rev. B 41, 4993.
Uozumi, T., Okada, K., Kotani, A., 1993. Electronic structures of Ti and V oxides: calculation of valence photoemission and Bremsstrahlung isochromat spectra. J. Phys. Soc. Jpn. 62, 2595.
Verleur, H.W., Barker, A.S., Berglund, C.N., 1968. Optical properties of VO2 between
0.25 and 5 eV. Phys. Rev. 172, 788.
Wentzcovitch, R.M., Schultz, W.W., Allen, P.B., 1994. VO2: Peierls or Mott–Hubbard?
A view from band theory. Phys. Rev. Lett. 72, 3389.